POLITECNICO DI TORINO
Repository ISTITUZIONALE

Experimental investigation of the effect of brick pattern on the structural response of masonry arches and barrel vaults

Original
Experimental investigation of the effect of brick pattern on the structural response of masonry arches and barrel vaults / Roselli, F.; Alforno, M.; Manuello Bertetto, A.; Venuti, F.. - In: CONSTRUCTION AND BUILDING MATERIALS. - ISSN 0950-0618. - 368:(2023). [10.1016/j.conbuildmat.2023.130434]

Availability:
This version is available at: 11583/2977536 since: 2023-03-28T12:23:26Z

Publisher:
Elsevier

Published
DOI:10.1016/j.conbuildmat.2023.130434

Terms of use:

This article is made available under terms and conditions as specified in the corresponding bibliographic description in the repository

Publisher copyright
Elsevier postprint/Author's Accepted Manuscript

© 2023. This manuscript version is made available under the CC-BY-NC-ND 4.0 license
http://creativecommons.org/licenses/by-nc-nd/4.0/.The final authenticated version is available online at:
http://dx.doi.org/10.1016/j.conbuildmat.2023.130434

(Article begins on next page)

06 May 2026

https://doi.org/10.1016/j.conbuildmat.2023.130434

Experimental investigation of the effect of brick pattern on the structural response of masonry arches and barrel vaults

F. Roselli[a], M. Alforno[b*], A. Manuello Bertetto[c], F. Venuti[a]

[a]Politecnico di Torino, Department of Architecture and Design, viale Mattioli 39, 10125 Torino, Italy
[b]University of Genoa, Department of Civil, Chemical and Environmental Engineering, Via Montallegro 1, Genova, Italy
[c]Politecnico di Torino, Department of Structural, Geotechnical and Building Engineering, corso Duca degli Abruzzi 24, 10129 Torino, Italy

*corresponding author: marco.alforno@edu.unige.it

Abstract.

In this study, an experimental campaign is carried out on 1:5 in-scale models of arches and barrel vaults built with different brick patterns (radial and vertical), to investigate their structural behaviour under settlement of the supports. Models are built with cement blocks and lime mortar joints. The arch models are tested under opening settlement of one support, whereas vaults are tested under shear settlement of one abutment. The three-dimensional deformations of the structures are acquired by image and video recording, 3D-Digital Image Correlation (DIC), close-range photogrammetry and structured light scanner. The influence of the brick pattern is investigated through comparison of crack patterns, ultimate displacements and failure mechanisms.

Keywords: *in-scale model; masonry; arch; barrel vault; brick pattern; support settlement.*

1 Introduction

For centuries, masonry represented the most employed construction technique in buildings, characterizing a great part of the western architectural heritage. Arches, and later vaults, represent the first overcome to the ancient trilithic system and for this reason they are two of the most used horizontal masonry structure typologies in historic buildings. As demonstrated by the recent seismic activity in the center of Italy, vaulted structures can respond to large support movements with the creation of plastic hinges with complex three-dimensional behaviour and cracking phenomena. However, the interpretation of the crack pattern is not

always straightforward, especially in three-dimensional vaulted structures, due to the great number of factors that influence the damage evolution. Among geometrical factors, recent numerical studies [1]-[11] have evidenced the key role of the brick pattern, namely the micro-geometry [12], on the global three-dimensional behaviour of vaulted structures. Despite the importance of this issue [8]-[10], there is a lack of experimental investigation on the topic.

Experimental tests have been widely used to study the stability of masonry arches and vaults by means of different experimental techniques, both quasi-static and dynamic. Because of the difficulties in performing full-scale tests on arches and vaults, experimental campaigns are usually performed on in-scale models, and only a very limited number of full-scale tests are available in the literature [13]-[15]. Small-scale models are less expensive and faster to be assembled, do not require significant building expertise, and allow to repeat several trials for the same test. Moreover, the use of reduced-scale models to simulate the structural behaviour of masonry constructions is also justified by Heyman's theory [16], since stability is a matter of geometry rather than material failure.

Since the strength of the materials of the models does not affect the behavior of curved structures, different materials, such as concrete, stainless steel, PVC, wood, and bricks, have been used for the blocks of small-scale arches and vaults, assembled either with mortar or dry joints.

The scope of experimental tests on in-scale models is to observe the structural response and collapse mechanism under different kinds of actions:

1. differential settlement of the abutments [17]-[34];
2. vertical external loads [22], [28],[29];
3. seismic action applied in quasi static regime, i.e., tilting plane, pulley systems, etc. [35]-[38];
4. seismic action applied in dynamic regime, i.e., shaking table tests [39]-[43].

Among the above-mentioned actions, differential settlements are one of the most recurrent causes of damage in masonry vaults, due to their high sensitivity to any small change in the boundary conditions. They are due not only to foundations settlements, but they can also develop during a seismic event. As a matter of fact, besides the dynamic response due to the acceleration of the vault's supports, a pseudo-static response is induced by the horizontal movement of the structures underneath (walls, columns) [26].

The present work aims to experimentally investigate the influence of the brick pattern on the in-plane shear response of barrel vaults. The shear test has been chosen since experimental campaigns devoted to pseudo-static response of masonry vaults to imposed shear displacements at the supports are quite scarce in literature [23], [24], [26]. In order develop a methodology that could be confidently applied to the test campaign on the barrel vaults, preliminary tests on a segmental arch subjected to a horizontal settlement of one support are carried out. This case study has been chosen since it is widely studied (e.g., [18], [19], [21], [22], [31]) and a great amount of data are available in literature for comparison and validation.

Two brick arrangements are considered: radial, with bed joints parallel to the spring lines, and vertical, with bed joints parallel to the head arches.

The paper develops through the following sections: Section 2 describes the geometry of the case studies, i.e., of the arch and vault models; Section 3 is dedicated to the description of the experimental set-up, in terms of testing devices, adopted materials and acquisition methodologies; Section 4 presents the results of the experimental campaign on the segmental arches and proposes a comparison with results from the literature; Section 5 discusses the experimental tests on the barrel vaults built with different brick patterns; finally, conclusions and perspectives are outlined in Section 6.

2 Geometry of the case studies

2.1 Segmental arch

The geometry of the segmental arch is described in Figure 1. The arch has a span length of 60 cm, a rise of 18.1 cm and an angle of embrace of 125°. The chosen dimensions mimic the ones of the head arches of the 1:5 in-scale cross vault built at the University of Genova [23].The arch is made of blocks of dimensions 9x20x40 mm, which mimic in scale 1:5 the dimensions of traditional masonry bricks.

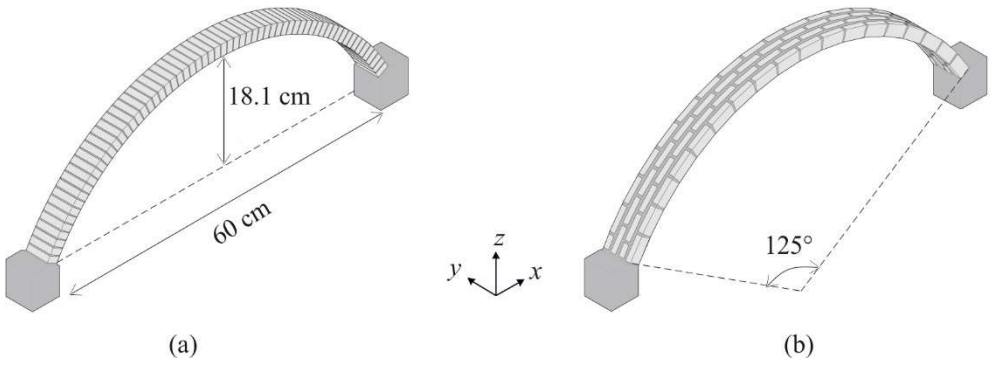

Figure 1: geometry of the segmental arch in the radial (a) and vertical (b) configuration

The bricks are arranged according to two patterns:

- a radial pattern (R), consisting in a single course of bricks (Figure 1a) disposed with the longitudinal dimension normal to the arch plane; the bricks are laid vertically on their short edge (rowlock orientation). With the use of this brick arrangement, the arch has a single type of transversal bed joints, wedge-shaped, laid between the major faces of the bricks. The final configuration of the arch models with radial pattern (denoted AR) involves the presence of 65 cement-based bricks each and wedge-shaped mortar joints with variable thicknesses between 1,3 mm and 1,9 mm.
- a vertical pattern (V), made of four parallel courses forming four parallel arches (Figure 1b), arranged so that both the arch thickness and the total arch depth are equal to the ones of the radial arch. Due to the presence of multiple rows of bricks, the bed joints are divided into two typologies: shorter transversal wedge-shaped joint, between each pair of bricks laying on the same arch, with measures between 1 and 2.8 mm, and longer longitudinal joint with rectangular cross-section, laying between each arch, with a

thickness of 5 mm. The configuration of the arches with vertical pattern (denoted AV) involves the presence of 74 cement-based bricks for each model organized in two couples of arches composed respectively of 18 and 19 bricks.

2.2 Barrel vault

The barrel vault has a square base: the net span of the vault is approximately 40 cm, the rise is about 12 cm, the length of the vault is 40 cm (Figure 2) and the angle of embrace is 125°. The rise-to-span ration is the same adopted for the arch model, but a smaller span has been preferred in order to reduce the number of bricks necessary to build the vault. The barrel vault is made of blocks of the same dimension as the arch blocks, arranged according to both radial (Figure 2a) and vertical pattern (Figure 2b). In the radial pattern, brick courses are laid normally with respect to the head arch plane, while the vertical pattern consists of adjacent arches with bed joints parallel to the head arch. In the following, the vault with radial and vertical pattern are referred to as VR and VV, respectively.

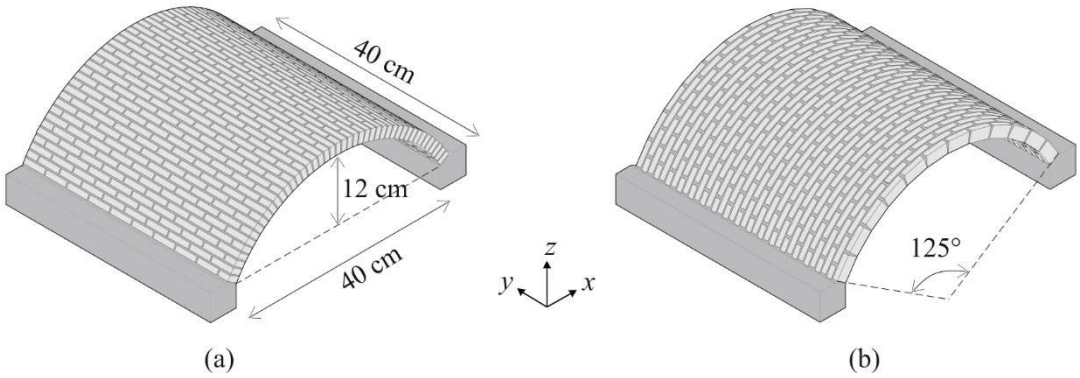

Figure 2: geometry of the barrel vault in the radial (a) and vertical (b) configuration

3 Experimental set-up

3.1 Testing devices

The testing device of the segmental arch was built in order to perform opening tests, i.e., to apply an imposed horizontal displacement in *x* direction at one of the abutments, while the other one remains fixed (Figure 3a). The centring is realized by a series of finnboard panels cut using CNC machines (Figure 3b). The lower surface of the centring is provided with three holes that fit into three threaded bars (centring supports in Figure 3a) attached to the testing device. These can be unscrewed in order to lower the centring after arch completion (Figure 3c) and to allow the removal of the centring (Figure 3d). Moreover, a digital calliper with a precision of a hundredths of a millimeter is installed at the moving abutment in order to measure the imposed displacement.

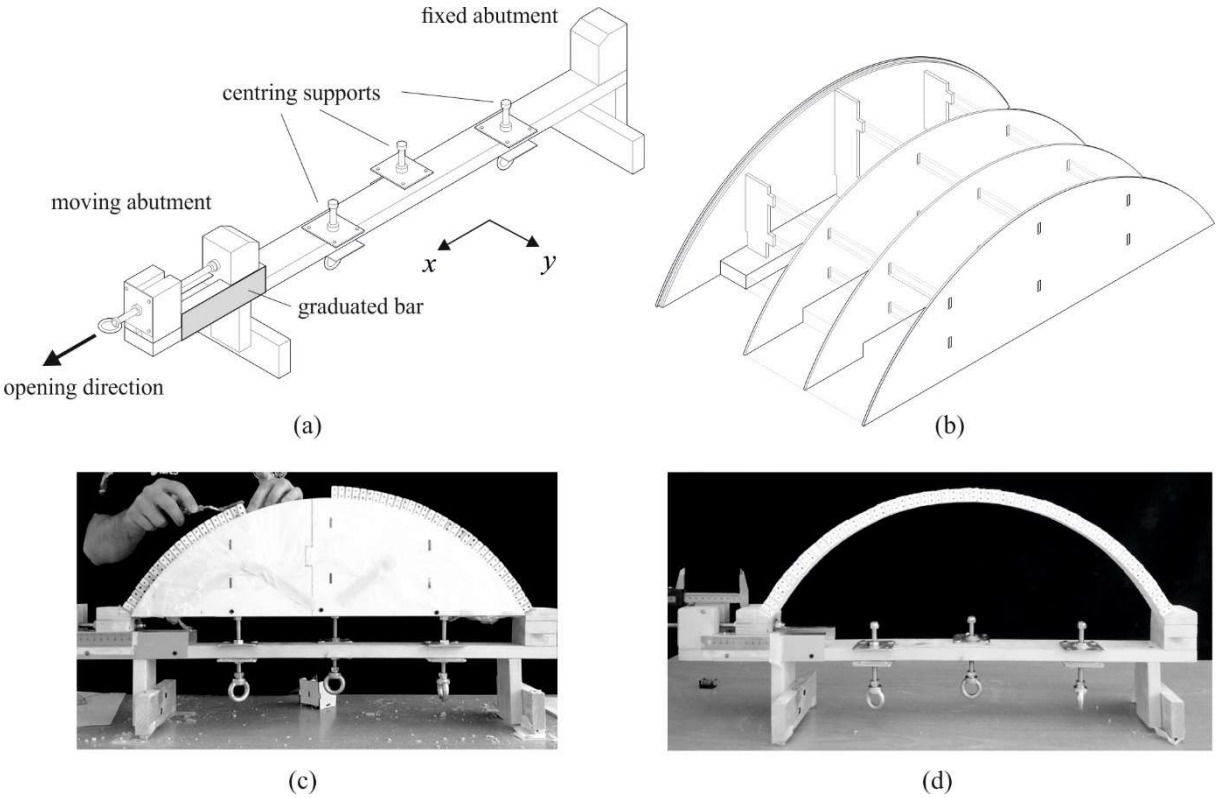

Figure 3: testing device of the segmental arch (a), axonometric exploded view of the centring (b), radial arch during construction (c) and after centring removal (d)

The testing device of the barrel vault was designed to allow both opening and shear tests to be performed (Figure 4a). Specifically, one of the abutments is fixed in the *x* direction and allowed to move in *y* direction, while the other abutment is fixed in the *y* direction and can be moved in *x* direction. The centring is designed, similarly to the arch centring, with a rigid base panel and an internal grid structure composed of several diaphragms (Figure 4b). Four threaded bars support the base of the centring, which can be lowered by unscrewing the bars to allow the centring removal after completion of the vault (Figure 4c-d).

The device is completed by a further equipment, used only during the construction of the vault with vertical pattern. It consists of a boundary vertical panel, fixed at one of the vault boundaries, against which successive brick courses make contrast by means of clamps (Figure 5). This solution avoids separation between subsequent courses and provides stability during construction thanks to the pre-compression exerted by the clamps. The latter is intended to replicate the construction procedure for real vaults with vertical pattern, in which parallel bricks are tapped in order to provide bonding in the direction transversal to the arch planes.

Imposed settlements are monitored through a digital calliper, with a precision of a hundredths of a millimeter, installed in correspondence of the moving abutment.

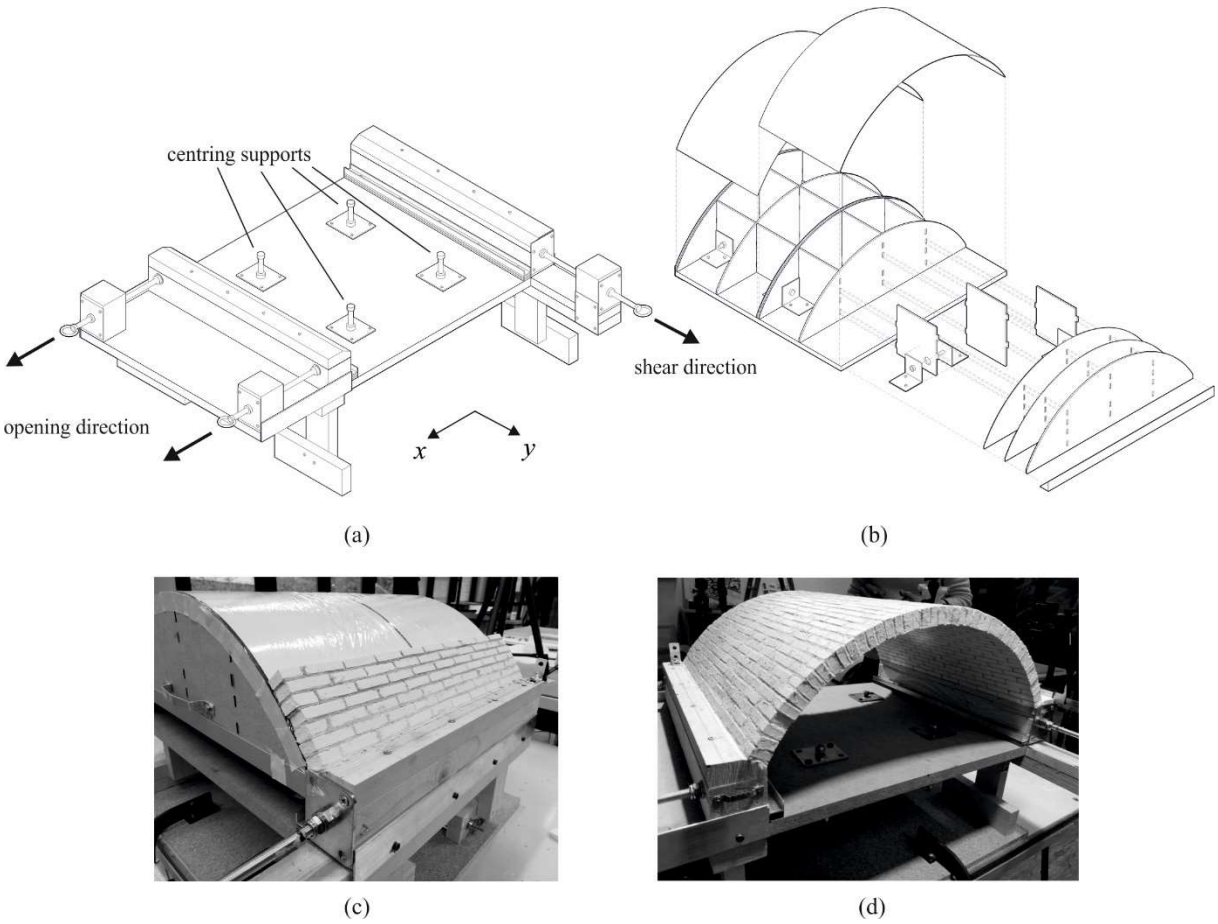

Figure 4: testing device of the barrel vault (a), axonometric exploded view of the centring (b), radial vault during construction (c) and after centring removal (d)

Figure 5: clamps adopted during the construction of the vault with vertical pattern.

3.2 Materials

The choice of materials was mainly dictated by the possibility to easily produce many units in a reduced amount of time and by the need to obtain a sufficient dimensional uniformity

158 between the blocks. According to these needs, two different materials were tested: wood and
159 cement, respectively.
160 The idea to use wooden blocks was inspired by previous research on in-scale models of
161 vaults, built with blocks and mortar [34]. Wooden blocks (Figure 6a) were obtained from 9
162 mm-thick and 20 mm-deep spruce laths, manually cut in pieces of 40 mm. The obtained blocks
163 were covered with a layer of enamel to reduce the absorption of water due to contact with wet
164 mortar. This solution was subsequently discarded since it presented several drawbacks. Firstly,
165 the hygroscopic behaviour of the spruce heavily altered the tests: despite the enamel treatment
166 the blocks tended to swell while in contact with the mortar, due to the high ratio between the
167 dimension of the joints and the bricks, modifying the whole geometry of the arch after drying.
168 This drawback has not been reported in other studies ([24], [34]), probably due to the higher
169 dimensions of the blocks. Moreover, the glaze-based (enamel) treatment altered the friction
170 properties in the mortar-wooden block joints. Secondly, the low density of the spruce blocks
171 made the arch quite unstable and heavily influenced by the vibrations derived from laboratory's
172 activity carried out in the surroundings.

173 (a) (b)

174 *Figure 6: wood (a) and cement (b) blocks*

175 To solve the abovementioned criticisms, cement blocks were fabricated. To this aim, a
176 formwork made of bicomponent silicon rubber was built by using 40 wooden blocks to obtain
177 the negative mould (Figure 7). This solution was chosen due to its reduced cost and ease of
178 casting and stripping. Different mixes of sand, cement and water were tested, before choosing
179 the one with the best performances in terms of regularity of the block surface and ease of
180 compaction of the casted material to avoid air bubbles inside the blocks. The chosen mix is
181 made of cement and water only, with 2:1 ratio. Stripping is made after 24 hours.

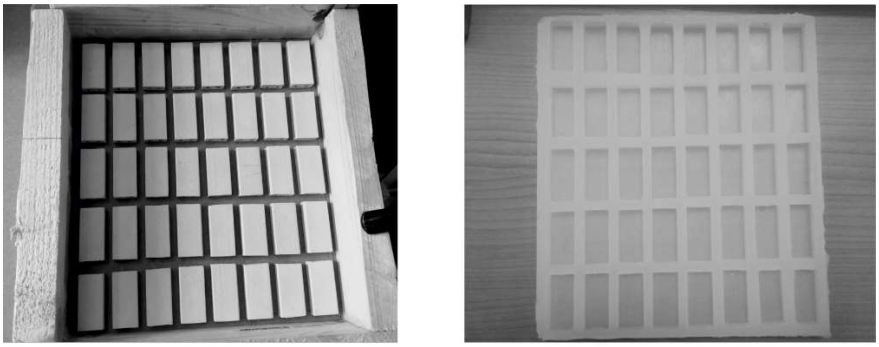

(a) (b)

Figure 7: Negative mould (a) and silicon rubber formwork (b)

The mix adopted for mortar is the same used by D'Altri at al. [24] in a 1:12 in-scale model of a gothic barrel vault. It is composed of 3 parts of Silica sand and 1 part of superventilated hydrated lime and by the addition of PVA glue and water. The adopted Silica sand has a particle size distribution classified as G_F85 according to UNI EN 12620 [44]. The PVA glue is added to improve workability and avoid fragmentation of the mixture. The quantity of water, not specified by the cited authors, was assumed equal to 1 part to obtain the required workability. The obtained mortar has weak cohesion, allowing cracks to open along the joints, as usually observed in historic masonry vaults.

3.3 Acquisition methodologies

The acquisition and postprocessing phases of the campaign have been managed through the integration of four methodologies:

1. simple image and video acquisitions (Figure 8a) performed by four synchronized GoPro Hero 5 session cameras distributed around the vault model;
2. Digital Image Correlation (DIC) (Figure 8b), performed with the DIC system Q400 from Dantec Dynamics A/S equipped with two convergent cameras;
3. close-range photogrammetry (Figure 8c) performed with a Canon EOS 60D camera and a Canon ef 24-105 mm f/4I lens;
4. range-based structured-light acquisition (Figure 8d) performed with a Stonex F6 SR scanner.

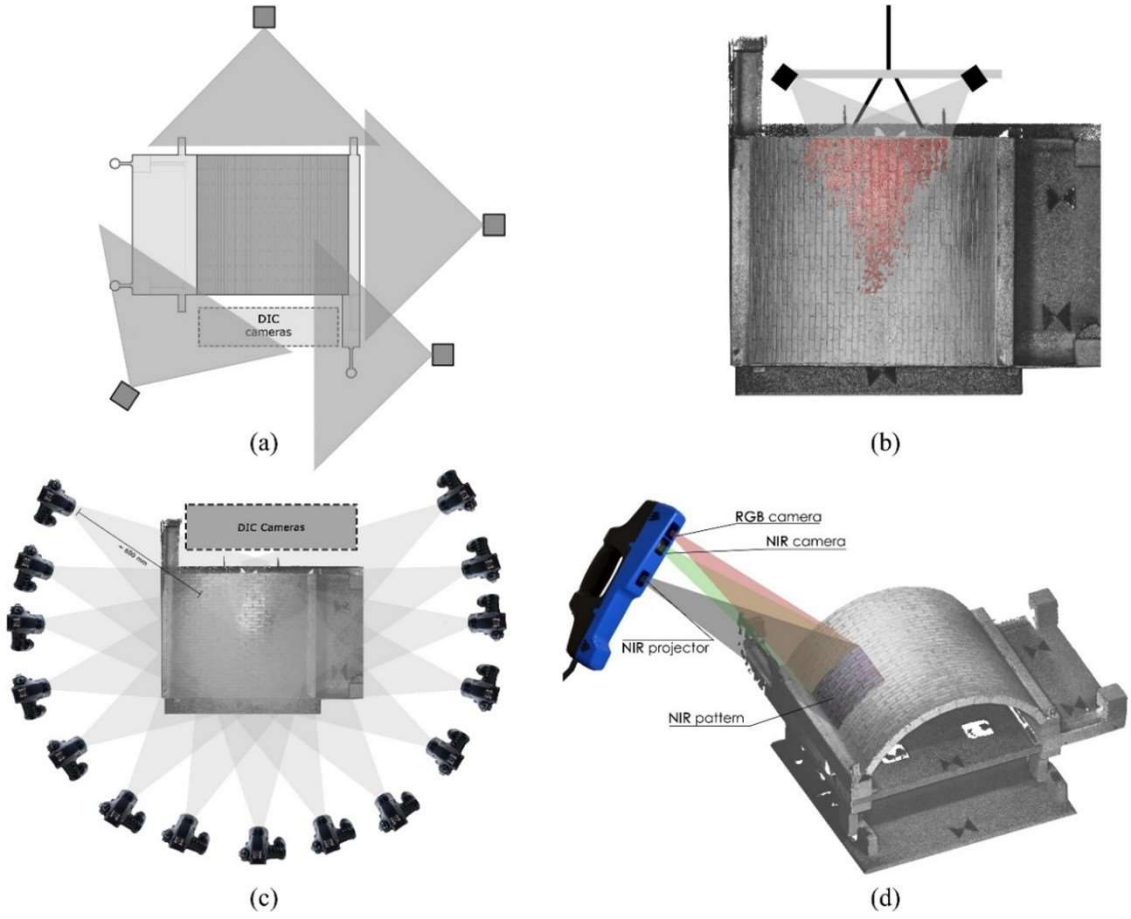

Figure 8: Summary of the adopted acquisition methodologies: (a) GoPro Hero 5 session cameras, (b) DIC cameras, (c) close-range photogrammetry, (d) range-based structured light scanning.

The Digital Image Correlation (DIC) [45] is part of the image-based techniques. Basically, DIC involves the comparison between a pair of stereoscopic images, taken as reference, with other pairs of images of the deformed object [46]. Cross-correlation is used to estimate strain and deformation of the tested object [45]. DIC works by tracking groups of pixels in the compared images. To allow for the pixel detection, the model is first covered by a layer of acrylic white paint and then by a black acrylic paint reproducing a texture of dots that act as targets.

Close-range photogrammetry uses one or more photographs of an object from different positions to derive its shape and location [47], through a three-dimensional reconstruction in digital or graphical form, based on inverse perspective and descriptive geometry [48].

The use of structure-light scanners offers good solutions in the contactless acquisition of small objects (magnitude < 1 m^3) [49][50]. These systems are based on the projection of specific patterns on the objects's surface and the consequent acquisition through an offset camera: using a principle similar to the triangulation is possible to estimate the position of physical points on the object by recording the deformation of the pattern [51].

The video acquisition provides interesting information about the behaviour of the models: videos are examined in slow motion and high-resolution frames are extracted to observe the

hinges evolution and the collapse mechanism. Close-range photogrammetry and structure-light scanners are adopted to obtain high-resolution 3D digital models of the structures in selected steps of the tests, used for metric documentation. The data processing of the close-range photogrammetry images is carried out to obtain dense point clouds comparable with the structured-light ones. The obtained three-dimensional point clouds (Figure 9) allow the extraction of orthophotos from the main planes of the in-scale models: these metric representations are extracted only from top and frontal views of the models, representing respectively the extrados and the head arch of the vaults, due to the impossibility to monitor the vault intrados. The obtained orthophotos are used to evaluate geometrical information such as the crack pattern and the magnitude of the structure's rotations. DIC is employed in this experimental campaign with the main objective of validating the results of image-based acquisition due to the fact that just a reduced portion of the vault is captured by the DIC cameras (Figure 8b).

The acquisitions are taken in different moments of the tests: a first one is done after the lowering of the centring, in the initial configuration of the model. The other acquisitions are taken during the imposition of the settlement. The tests are stopped to allow the acquisition procedures.

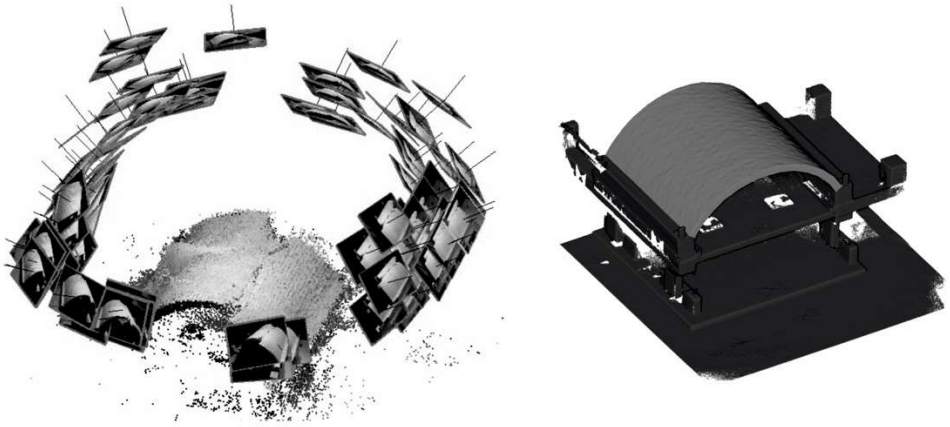

Figure 9: raw point cloud derived from close range photogrammetry (a) and final segmentation of the cloud (b).

4 Results of tests on the segmental arch

The experimental tests on the segmental arch were performed with the aim of developing a work methodology, that could be confidently applied on the subsequent test campaign on the barrel vaults. Specifically, these preliminary tests allowed to select the most proper materials and technique for building and assembling the blocks. The test involves the movement of one of the abutments along the longitudinal direction (x) by twisting a threaded rod, while the other support is fixed to the testing device (Figure 10).

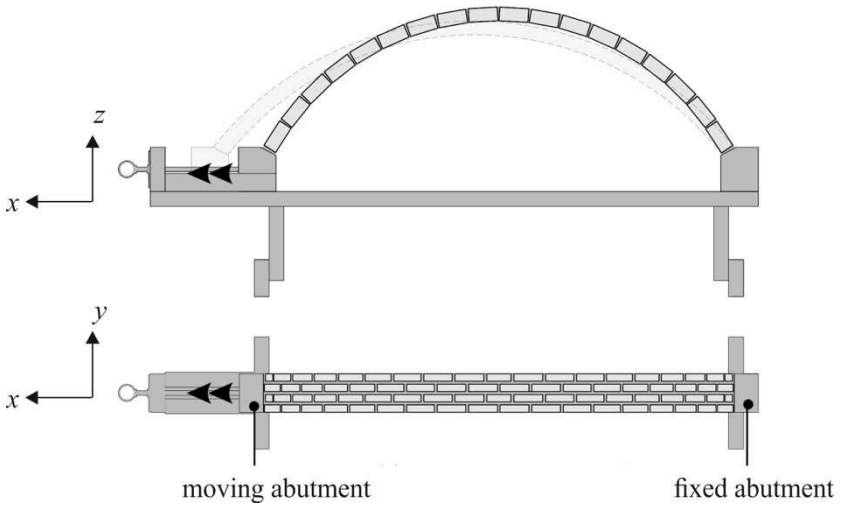

Figure 10: Schematic description of the opening displacement imposed to the arch models.

The movement of the abutment is constantly monitored with a digital calliper, so the ultimate displacement (u_u) is recorded for each test. Images of the models are acquired at steps of 1 mm of imposed displacement, temporarily stopping the test. The photographic acquisition provides images of the model during the deformation, allowing to monitor the hinge opening during each step of imposed displacement. Moreover, the video acquisition allowed to capture the failure mechanisms of the models. In virtue of the bidimensional typology of the structures, all the data are extracted from the main vertical plane of the arches (*x*-*z*).

The opening displacement imposed during the tests leads to the failure of the arch models, with the formation of cracks along the joints, assumable as hinges: the arch deformation during the test allows the shape accommodation through a maximum of three hinges, while the structure remains stable. The theoretical failure mechanism must appear with the formation of the other two hinges simultaneously, for a total of five, to transform the stable structure into a symmetric mechanism ([30],[21]). Despite this theoretical assumption, in reality little asymmetricity in the arch construction can lead to imperfect asymmetrical mechanisms, triggered by the opening of just a fourth hinge ([16], [17], [19], [21], [22], [30]) as actually observed in the performed tests. The collapse mechanism is recorded, along with the hinge position (Figure 11 and Figure 12) and the value of ultimate displacement (Table 1).

Table 1: ultimate displacements u_u [mm] on radial (AR) and vertical (AV).

AR_1	AR_2	AR_3	AR_4	AR_5	AV_1	AV_2	AV_3
13.2	13.95	16.14	13.91	13.15	10.62	16.70	29.32

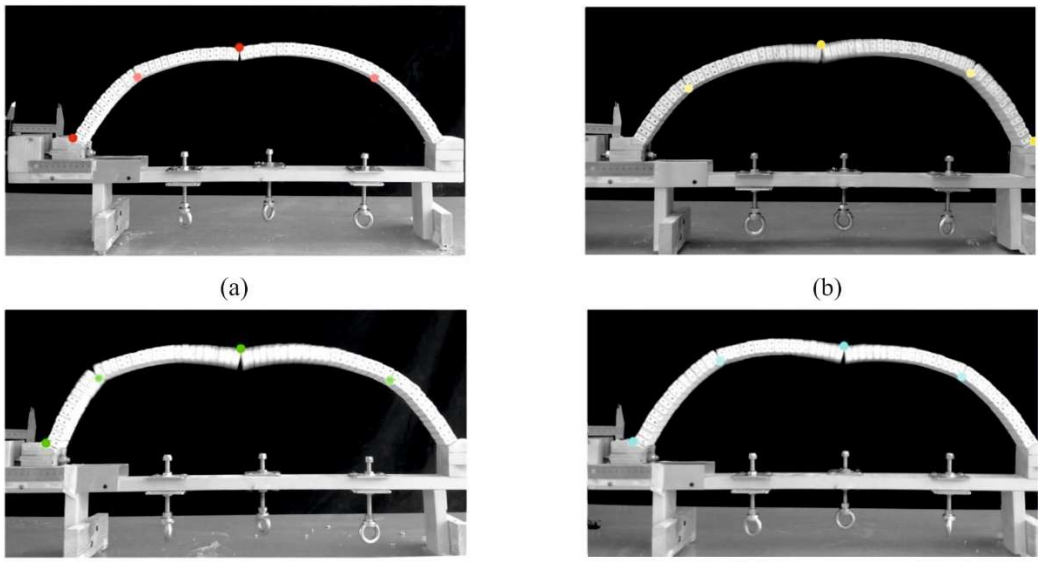

(a) (b) (c) (d)

Figure 11: Collapse shapes and hinge position in AR_2 (a), AR_3 (b), AR_4 (c) and AR_5 (d).

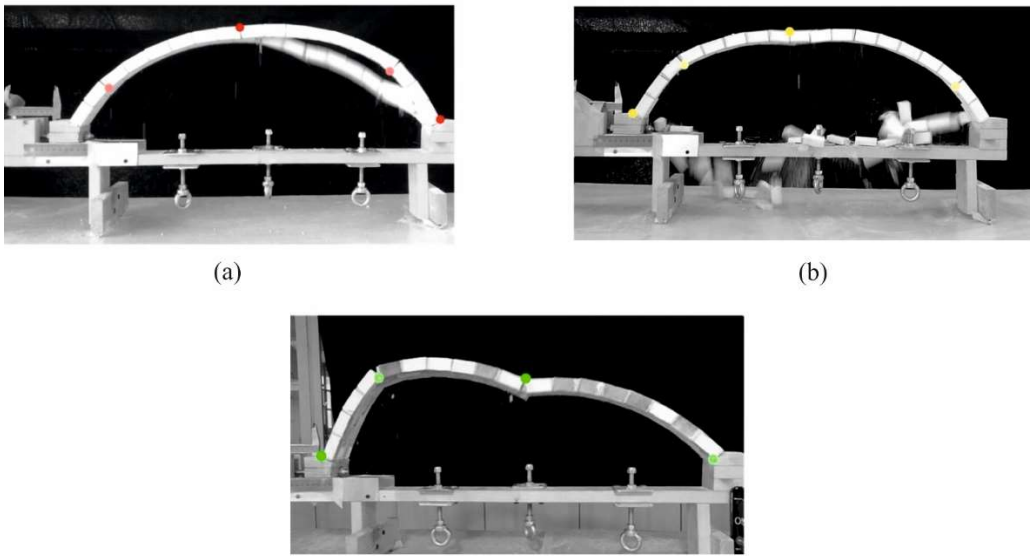

(a) (b) (c)

Figure 12: Collapse shapes and hinge position in AV_1 (a), AV_2 (b), AV_3 (c).

All the recorded collapse mechanisms are characterized by four hinges, with an alternation in the position of the last one at the abutments, in accordance with the other experimental and analytical investigations on this topic [30]. In particular, in the tests on AR_1, AR_3, AR_4, AV_2, and AV_3 models, the fourth hinge that induces collapse is located at the moving abutment, whereas in the AR_2 and AV_1 models it is located at the fixed abutment. It is worth noticing that, despite the different discretization of the arch geometry deriving from the two different brick arrangements, the hinge positions fall into similar circular sectors (described by α_1, α_2, α_3, as shown in Figure 13).

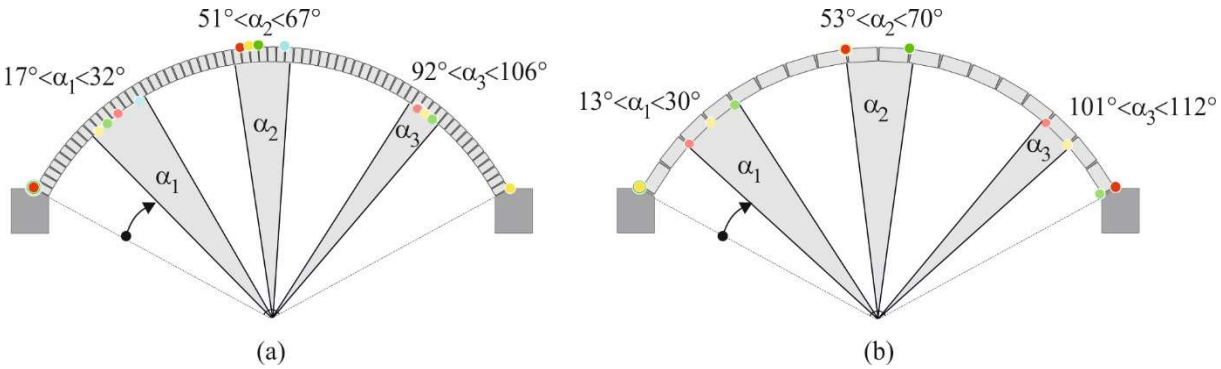

Figure 13: Range of angles in which the hinges develop in AR (a) and AV (b) models.

The performances of AR and AV models are quite different both in terms of ultimate displacements (Table 1) and of collapse shapes (Figure 11 and Figure 12). The ultimate displacements recorded in the AR models are not as dispersed as in the AV models. Moreover, the three AV models also show different behaviour at collapse. This variation can most likely be linked to the construction procedure: after the first trials with the vertical arrangement, it was noticed that the parallel arches separated at an early stage of imposed displacement, leading to differential collapse mechanisms of subsequent brick rows (Figure 12a). To avoid this issue, the construction process of the AV models was modified by imposing a small amount of pre-compression between the longitudinal mortar joints that bond the different arches together. As a result, the ultimate displacement has meaningfully increased in the two models tested after this variation (AV_2 and AV_3). The collapse mechanism also shows a variation after the change in the construction process, with the absence of differential failures of the successive arches (Figure 12cFigure 16).

Table 2: Comparison of experimental results on segmental radial arches subjected to opening settlement.

Authors	**Blocks**	**Joints**	***L*** **[mm]**	***t*** **[mm]**	***f*** **[mm]**	***R*** **[mm]**	***α*** **[°]**	***t/L*** **[-]**	***t/R*** **[-]**	u_u/L **[%]**
Romano, 2005 [33]	concrete	dry	908	60	348	500	150	0.066	0.120	7.61
			879	90	337	500	150	0.102	0.180	12.5
			814	60	235	500	120	0.074	0.120	8.43
			788	90	227	500	120	0.114	0.180	14.12
			910	90	455	500	180	0.099	0.180	7
Ochsendorf, 2006 [19]	cast concrete	dry	390	50	195	220	180	0.128	0.227	15.4
			709	50	297	385	160	0.071	0.130	7.8
Shapiro, 2012 [22]	3D printed	dry	313	24	100	185	130	0.077	0.130	7.5
			283	24	74	185	110	0.085	0.130	9.4
Alforno, 2020 [17]	timber	lime mortar	600	20	182	348	125	0.033	0.057	2.1
Masciotta, 2020 [21]	brick	lime mortar	1900	75	430	1301	97	0.039	0.058	6.3
Ferrero, 2022 [31]	composite material	dry	533	24	162	312	125	0.045	0.077	3.7
Present study	cement	lime mortar	600	20	182	348	125	0.033	0.057	2.2

The results obtained on the arches with radial pattern can be compared with the ones from other similar experimental tests in the literature. Table 2 summarizes the main features of experimental tests on segmental arches subjected to opening settlement (see Figure 14a for explanation of the geometrical parameters reported in the table) along with the ultimate imposed displacement, corresponding to the arch collapse, scaled with respect to the arch span length (u_u/L). For a better reading, Figure 14b plots u_u/L versus the thickness to span ratio t/L. Results from the present study are represented by a red circle.

The graph in Figure 14b shows a quite perfect linear dependence of u_u/L on the thickness to span ratio t/L, whichever the material adopted to build the blocks, whichever the angle of embrace α and for both cases of dry and mortar joints. The only outlier corresponds to the test described in [21] and is due to the fact that, in that case, the arch was not subjected to its dead load only, but two additional weights were positioned at the haunches to simulate the effect of infill: in this case the stabilizing effect of the infill induces an increase of the displacement capacity. The results obtained in the present experimental campaign are in perfect agreement with the trend discussed above.

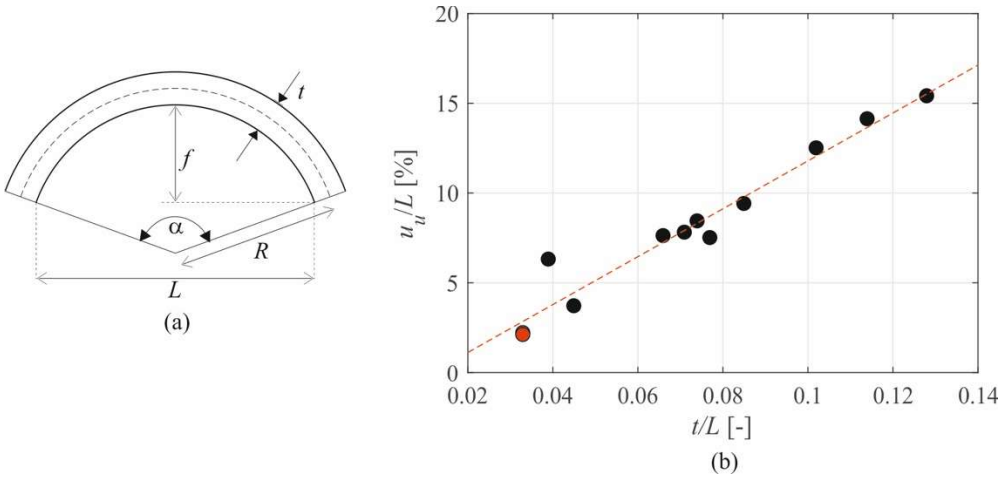

Figure 14: Scheme of geometrical parameters (a) and ultimate displacement vs t/L.

5 Results of tests on the barrel vaults

The vault models are tested under in-plane shear displacement imposed to one of the abutments. Two models for each brick pattern are built and tested until collapse. The test is performed by imposing the sliding of one support along the longitudinal direction *y*, (Figure 15) and the imposed displacement is constantly monitored through a digital calliper.

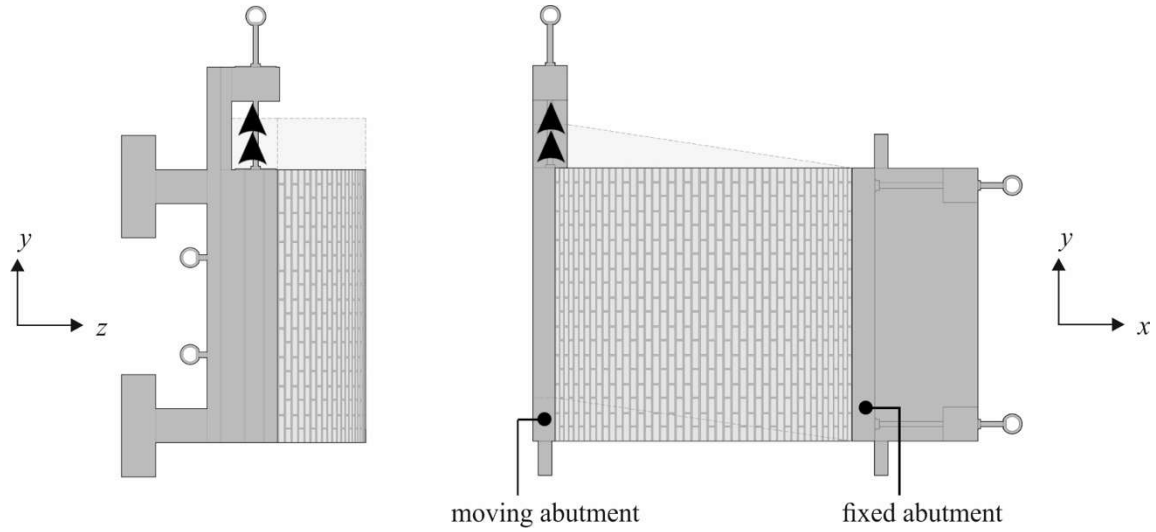

Figure 15: Schematic description of the shear displacement imposed to the vault models.

The test is stopped to perform the acquisition of the deformed shapes, through close range photogrammetry and structured light, at selected imposed displacements to allow comparison between the different models. Moreover, the acquisition process is repeated every time a significant phenomenon, such as crack openings, rotations, local failure, occurs. Figure 16 reports a synoptic scheme of the acquisition steps as a function of the imposed displacement u_y for each vault. It is worth noting that the acquisition steps are coincident in the case of vaults with the same brick pattern, but not always coincident between VR and VV vaults, since they have not been set *a priori* but on the basis of the visible phenomena observed during the test.

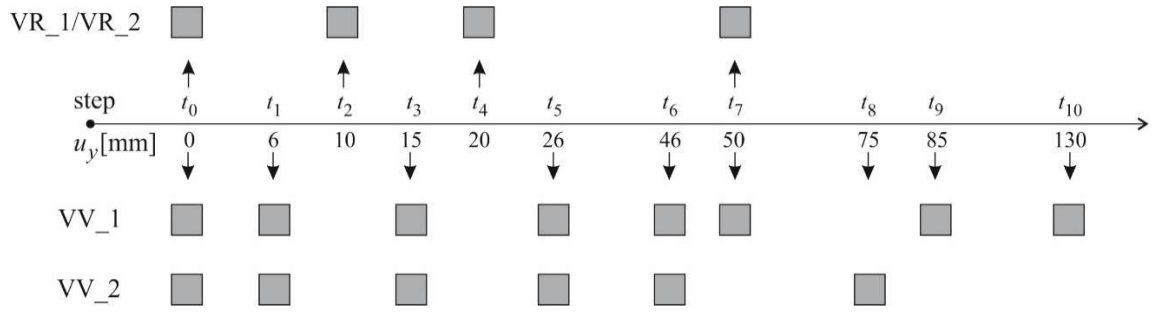

Figure 16: Synoptic scheme of the acquisition steps.

In Figure 17 a selection of images of the failure, from the most representative perspective, is reported, while Table 3 summarises the ultimate displacement u_u reached in each test.

Table 3: ultimate displacements u_u [mm] of barrel vaults

VR_1	VR_2	VV_1	VV_2
60.67	91.42	>150	93.77

Differently from arches, vaults involve complex three-dimensional failure mechanisms.

The VR models show shear cracks that run across the whole depth of the model following the longitudinal joints. Some of these evolve into rotational hinges and trigger a global collapse mechanism. However, the two models reach the collapse at quite different ultimate displacements (Table 3). On the contrary, the VV models are characterized by the local collapse of some arches near the heads of the vault and by the rigid rotation of the remaining portions. The rigid rotation of the vault on the abutment is particularly evident in the VV_1 model, which reaches the end of displacement range (fixed at 150 mm) without a global failure. Local collapses make it difficult to identify the displacement capacity in the VV vaults, therefore the ultimate displacements reported in Table 3 should be carefully interpreted.

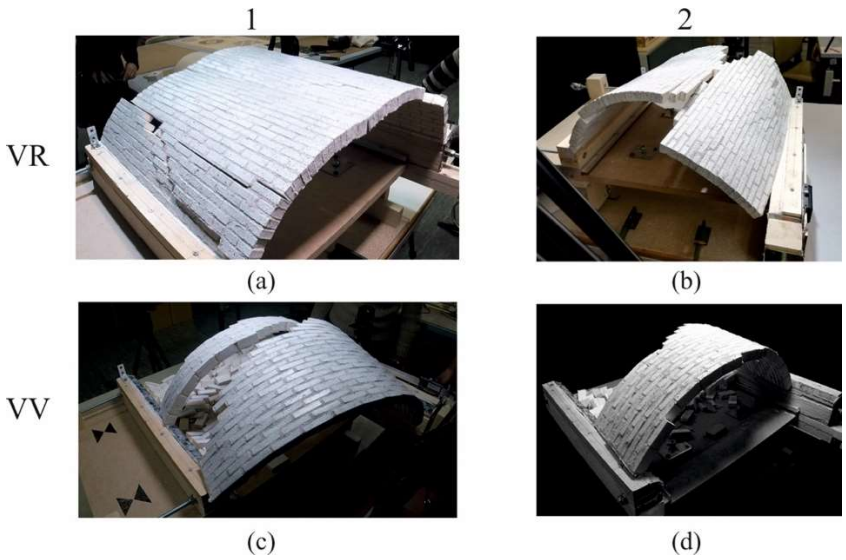

Figure 17: collapse mechanisms of the tested models: VR_1 (a), VR_2 (b), VV_1 (c) and VV_2 (d)

The reliability of the data obtained by the close-range photogrammetry is preliminarily assessed by comparing the results obtained through point clouds with the results from the DIC. The comparison is performed on VR_1 vault by evaluating the y component of the displacement vector Δy for a selected point P on the extrados (Figure 18a) at each acquisition step (t_2, t_4, t_7 that correspond to steps 100, 200, 500 of the DIC acquisition process, respectively). Figure 18b plots the time history of Δy obtained through DIC and the instant values of Δy_i extracted from point clouds comparison at the three selected acquisition steps, where Δy_i is given by the distance between point P at steps t_i and t_0 (i=2,4,7). The comparison shows a shift of about 1-2 mm between the two data sets. This error is considered acceptable, considering the manual selection of point P at the different steps.

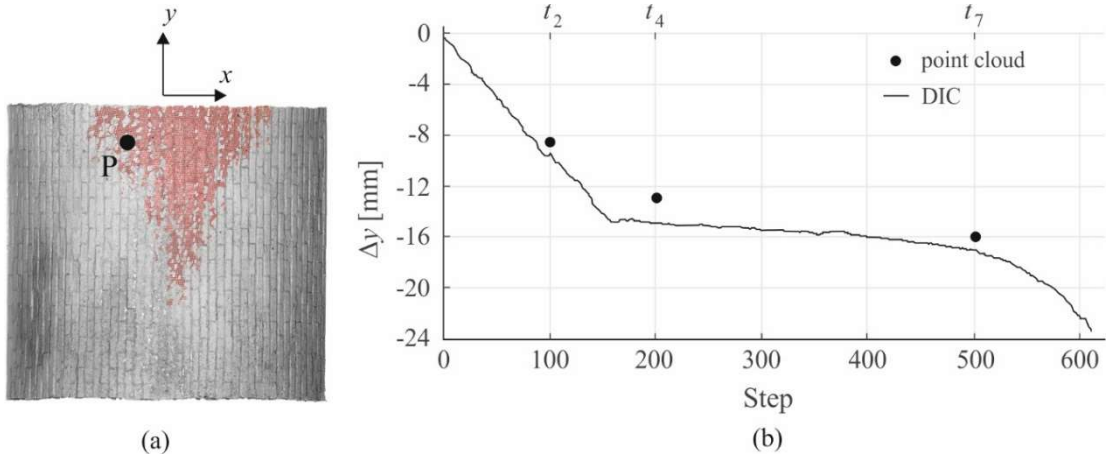

Figure 18: Position of point P on the vault extrados (a) and its displacement acquired through DIC and point cloud comparison

A further comparison between data collected through different techniques is provided in Figure 19 for the VR_1 vault, as an example. In particular, Figure 19 compares the macroscopic visible phenomena reconstructed by direct observation, video acquisition and three-dimensional data managing of the range-based and image-based acquisition techniques (Figure 19b top) with the time history of the mean displacement of a control linear strain-gauge (Figure 19a) recorded through DIC (Figure 19b bottom). This comparison shows a perfect match between phenomena recorded with different techniques. Specifically, the mean displacement linearly increases until u_y of about 16 mm, corresponding to the opening of the inclined longitudinal crack that separates the right haunch portion. Then, the mean displacement remains almost constant and start increasing again in correspondence of the step (about 51 mm) when the structure starts rotating until collapse.

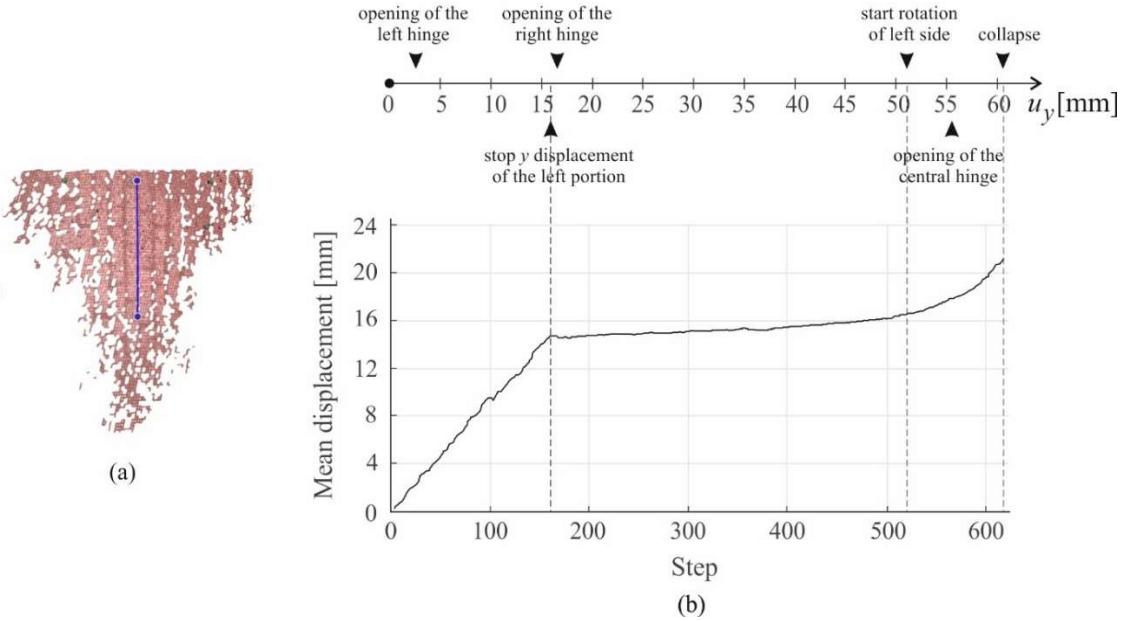

Figure 19: Position of the linear strain-gauge (a), time history of mean displacement of the linear strain-gauge on the VR_1 vault (b)

Crack patterns are obtained by merging information from synchronized video acquisition, dense point clouds and visible phenomena observed during the test development. They are illustrated in Figure 20 on the orthophotos of the vault extrados for each acquisition step. Collapsed portions of the vaults are highlighted by red or blue solid color.

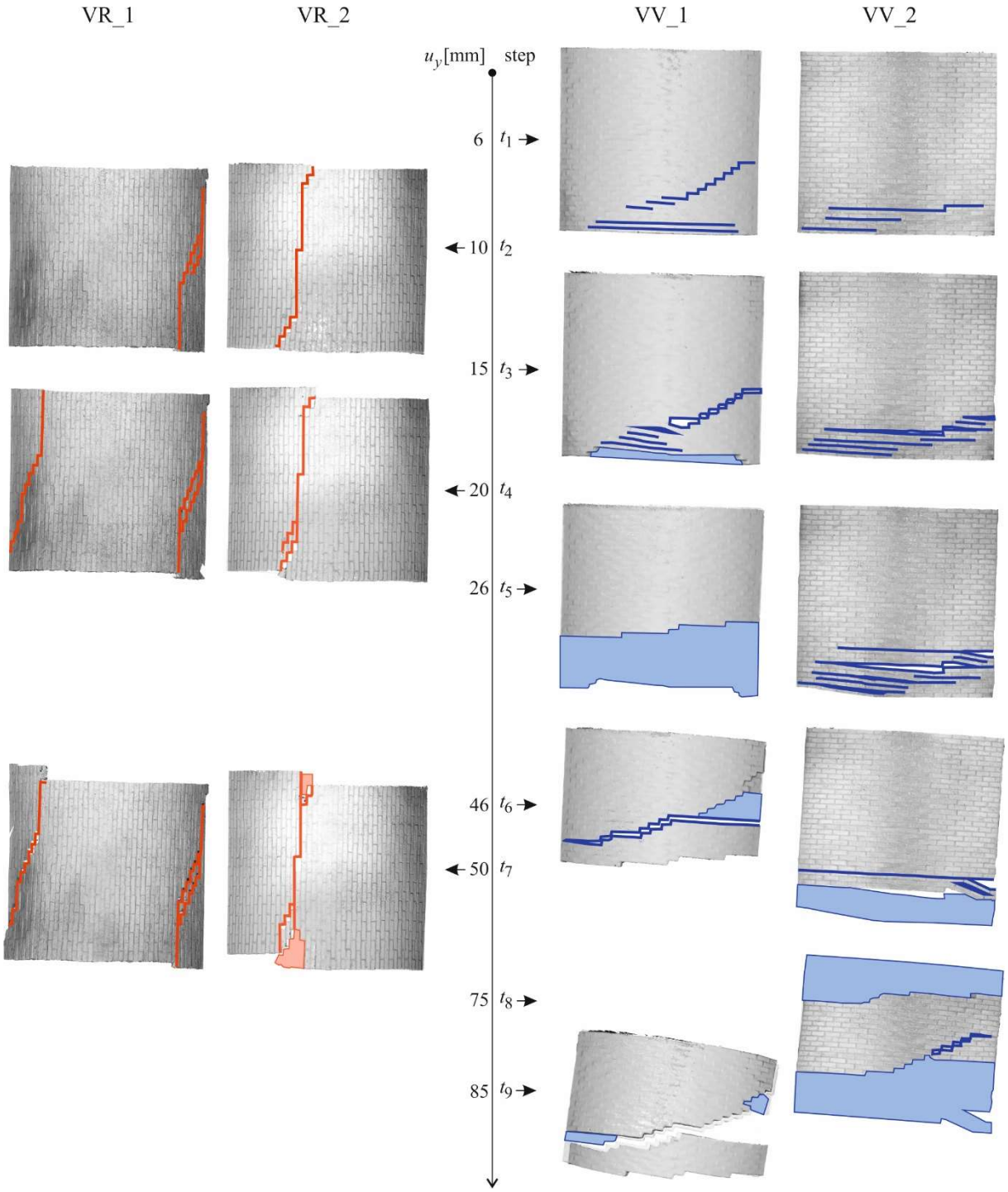

Figure 20: Crack patterns in radial (VR) and vertical (VV) vaults.

The critical analysis of the crack patterns experienced in the models reveals substantial differences between the two brick arrangements. Characteristic crack patterns are summarized in Figure 21, which compares VR_1 and VV_1 at step t_7 (u_y = 50 mm). In the VR models most of the cracks occur along the longitudinal joints. These major cracks appear to be quite straight along a single longitudinal joint or inclined involving multiple rows of bricks (Figure 20, left side, Figure 21a). A similar crack pattern was obtained by D'Altri et al. [24] on a scaled model of a pointed barrel vault built with a radial pattern. On the other hand, in the VV models the major cracks occur in the radial joints, leading to the formation of separate portions of the structure (Figure 20, right side, Figure 21b) that lead to local collapses of the portions near the head arches. The major cracks can assume either straight or inclined directions also in VV models, reasonably depending on construction issues. These results are in perfect agreement with those reported by Alforno [52], where a numerical study on ideal barrel vaults subjected to shear settlement of the abutments was performed (Figure 22): the radial vault collapses with a four-hinge mechanism due to the formation of longitudinal and inclined cracks; the vertical vault undergoes local collapses of the portions near the head arches (see [17] for a detailed description of the adopted numerical approach, which is out of the scope of this paper). Even though the geometry of the ideal barrel vault differs from the one object of the present study, it is worth noting that also in the reported numerical investigation the vault with vertical brick pattern showed a higher displacement capacity than the one with radial arrangement.

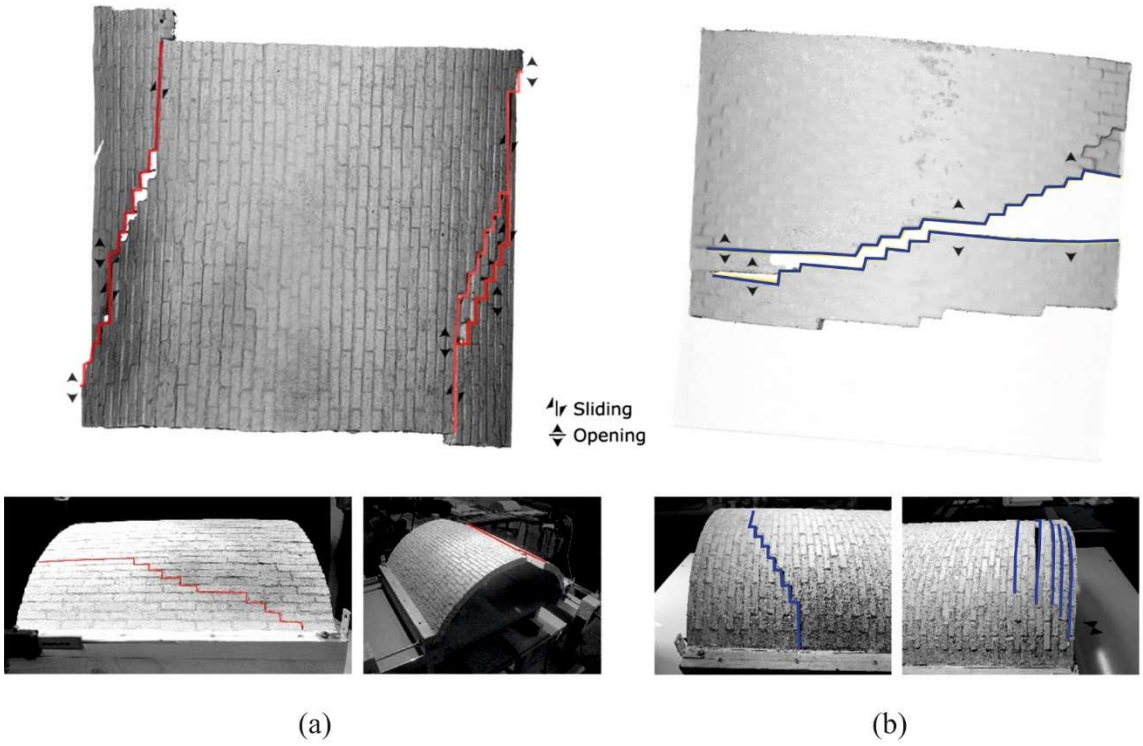

Figure 21: Characteristic crack pattern of VR (a) and VV (b) vaults

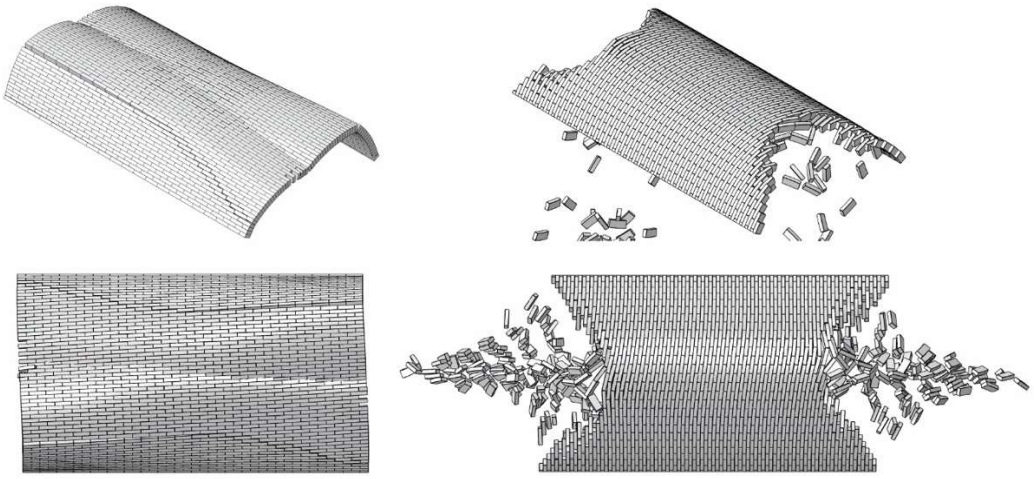

Figure 22: Deformed shapes of radial (a) and vertical (b) barrel vaults according to Alforno [52]

Besides the described main differences in the crack pattern between vaults arranged with different brick apparatus, some differences occur between vaults arranged with the same brick laying technique, as clearly visible in Figure 20 for the VR_1 and VR_2 vaults. Specifically, the major crack position varies due to construction issue, i.e., to the impossibility to perfectly replicate the model construction. These construction imperfections are expected to be much greater in building in-scale models than real scale vaults. In the VR_1 vault the two major cracks lead to the separation of the central portion, that starts rotating upon the sliding haunches; in the VR_2 model, the major crack along the key joint causes sliding between the two separated portions, with consequent small local failures near the heads and the rigid rotation of the two haunches upon the abutment. This difference in the collapse mechanism induces quite different displacement capacity, being the ultimate displacement of the VR_2 vault 50% higher than the one of the VR_1 vault.

Finally, rotations of the vault longitudinal axis with respect to the original configuration (t_0) are measured and plotted in Figure 23 for all the analyzed specimens. Linear fits of the data for VR and VV vaults allows a general trend to be outlined. Specifically, the VR vaults experience lower rotations with respect to the VV vaults. This is due to the different crack patterns described above: in the VR vaults the longitudinal cracks foster sliding in y direction between separated portions of the vault; conversely, transversal cracks and subsequent local collapses in the VV vaults cause rotation of the remaining portion of the vault in the x-y plane.

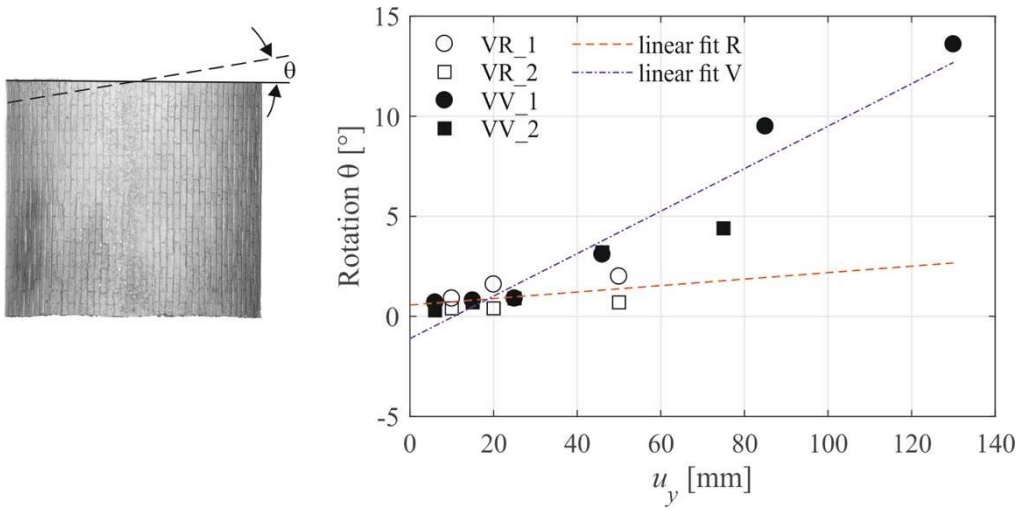

Figure 23: Rotation with respect to initial geometry versus imposed displacement

It is worth pointing out that the results of the present experimental campaign are not statistically relevant due to the small number of performed tests (two for each brick arrangement). The large scattering of the quantitative results is expected to decrease for a higher number of specimens. Therefore, in order to acquire reliable quantitative data necessary to confidently calibrate numerical models, the experimental campaign must be extended. Hence, the present work has to be intended as a first exploratory study which results can offer qualitative interpretation of the influence of the brick pattern on the collapse mode.

6 Conclusions

This paper presents the results of an experimental campaign addressed to investigate the effect of brick pattern on the static behaviour of segmental arches and barrel vaults subjected to opening and shear settlement of the abutments. Two brick arrangements have been considered: radial, with bed joint perpendicular to the head arches, and vertical, with bed joints parallel to the head arch plane.

Tests performed on arches with opening settlement of one support allow the following conclusions to be outlined:

- Radial arches (AR) present collapse shapes and ultimate imposed settlement in line with other experimental data in the literature. Specifically, a linear relationship between the dimensionless ultimate displacement and the thickness to span ratio was found to hold for segmental arches subjected to their own weight, whichever the adopted materials and angle of embrace, with both dry and mortar joints;
- Vertical arches (AV) display ultimate displacement strongly dependent on the construction methodology. In particular, they can reach a significant higher displacement capacity (up to twice the one of AR) if pre-compression is applied between the longitudinal mortar joints that bond the different arches together.

Results of the tests on barrel vaults subjected to shear settlement of one support highlight the following issues:

- The crack pattern is strongly influenced by the brick arrangement. Radial vaults (VR) are characterized by major cracks along the longitudinal joints with consequent sliding of the separated portions of the vault in the direction of imposed settlement; vertical vaults (VV) show major cracks along the radial joints, with partial collapse of the head arches and rotation of the remaining part of the vault in the horizontal plane;
- Construction imperfections strongly influence the collapse shape and the displacement capacity, leading to different results for the vaults with same brick pattern;
- in general, the VV vaults under shear settlement display a higher ultimate displacement than the VR vaults. The same holds for AV arches under opening settlement in presence of transversal pre-compression.

To the Authors' knowledge, the described experimental campaign is the first specifically addressed to investigate the effect of the brick pattern. The obtained preliminary results qualitatively confirm previous findings of numerical studies described in [52] and the importance of this construction issue on the static behaviour of arches and vaults. A deeper knowledge of this topic can help in choosing the most proper strengthening technique in line with the "minimum intervention" approach recommended for historic constructions.

Future research will be addressed to extend and improve the experimental campaign so as to: overcome the discussed construction issues; provide physical-mechanical characterization of the adopted blocks and mortar; allow for higher level of repeatability of the tests; employ load cells to measure reaction forces; improve the acquisition methodologies in order to have a continuous monitoring of the displacement field of the entire surface of the vault. These future results can be used to validate numerical models, which can be subsequently confidently adopted to extend the investigation to other kinds of vaulted structures.

CRediT author contribution statement

Francesco Roselli: Methodology, Validation, Investigation, Formal analysis, Visualization, Writing - Review & Editing. **Marco Alforno**: Conceptualization, Methodology, Validation, Formal analysis, Writing - Original Draft, Writing - Review & Editing, Supervision. **Amedeo Manuello**: Resources, Writing - Review & Editing. **Fiammetta Venuti**: Conceptualization, Methodology, Resources, Validation, Formal analysis, Visualization, Writing - Original Draft, Writing - Review & Editing, Supervision.

ACKNOWLEDGEMENTS

F. Chiabrando, A. Spanò, G. Sammartano and G. Patrucco (Politecnico di Torino, Department of Architecture and Design) are greatly acknowledged for the photogrammetric and laser scanner survey of the models as well as for the support in postprocessing of data.

REFERENCES

[1] Calderini, C., S. Lagomarsino. 2004. The effect of the masonry pattern on the global behaviour of vaults. In *Proceedings of the 4th International Conference on Structural Analysis of Historical Constructions* (Padova, Italy).

[2] Barbieri, A., C. Carloni, A. Di Tommaso. 2004. Masonry orthotropic vaults in historical construction: the herring-bone pattern. In *Proceedings of the 4th International Conference on Arch Bridges ARCH 04* (Barcelona, Spain).

[3] Baratta, A., O. Corbi. 2012. The static behavior of historical vaults and cupolas. *Journal of Heritage Conservation*, 32: 65-81.

[4] Foraboschi, P. 2014. Resisting system and failure modes of masonry domes, *Engineering Failure Analysis*, 44: 315-337. DOI: 10.1016/j.engfailanal.2014.05.005.

[5] Foti, D., V. Vacca, I. Facchini. 2018. DEM modeling and experimental analysis of the static behavior of a dry-joints masonry cross vaults. *Construction and Building Materials*, 170:111–20. DOI: 10.1016/j.conbuildmat.2018.02.202.

[6] Alforno, M., Venuti, F., Monaco, A., Calderini, C. 2021. Numerical investigation of the influence of constructive aspects on the structural behaviour of masonry cross vaults. *International Journal of Architectural Heritage*. DOI: 10.1080/15583058.2021.1992534.

[7] Chen, S., A. Ferrante, F. Clementi, K. Bagi. 2021. DEM analysis of the effect of bond pattern on the load bearing capacity of barrel vaults under vertical loads, International *Journal of Masonry Research and Innovation*, 6(3):346, DOI: 10.1504/IJMRI.2021.116234

[8] Breymann, G.A. 1849. Allgemeine Bau-Constructions-Lehre, mit besonderer Beziehung auf das Hochbauwesen. Vol. 1, *Constructionen in Stein*. Hoffmann, Stuttgart.

[9] Choisy, A. 1883. *L'art de batir chez les Byzantines*. Société anonyme de publications périodiques, Paris.

[10] Wendland, D. 2007. Traditional vault construction without formwork: masonry pattern and vault shape in the historical technical literature and in experimental studies. *International Journal of Architectural Heritage*, 1(4): 311-365. DOI: 10.1080/15583050701373803.

[11] Boni, C., D. Ferretti, E. Lenticchia. 2021. Effects of Brick Pattern on the Static Behavior of Masonry Vaults, *International Journal of Architectural Heritage*, DOI:10.1080/15583058.2021.1874565.

[12] Alforno, M., F. Venuti, A. Monaco. 2020. The structural effects of micro-geometry on masonry vaults, *Nexus Network Journal*, 22: 1237–1258. DOI: 10.1007/s00004-020-00499-9.

[13] Giamundo, V., G.P. Lignola, G. Maddaloni et al. 2016. Shaking table tests on a full-scale unreinforced and IMG-retrofitted clay brick masonry barrel vault. *Bulletin of Earthquake Engineering*, 14: 1663– 1693. DOI:10.1007/s10518-016-9886-7.

[14] Torres, B., E. Bertolesi, P. A. Calderón, J. J. Moragues, J. M. Adam. 2019. Experimental investigation of a full-scale timbrel masonry cross vault subjected to vertical settlement. *Construction and Building Materials*, 221: 421–32. DOI: 10.1016/j.conbuildmat.2019.06.015

[15] Torres, B., E. Bertolesi, P. A. Calderón, J. J. Moragues, and J. M. Adam. 2019. A full-scale timbrel cross vault subjected to vertical cyclical displacements in one of its supports. *Engineering Structures,* 183: 791-804. DOI: 10.1016/j.engstruct.2019.01.054.

[16] Heyman J. The stone skeleton. Cambridge University Press; 1995.

[17] Alforno, M., A. Monaco, F. Venuti, C. Calderini. 2020. Validation of simplified micro-models for the static analysis of masonry arches and vaults, *International Journal of Architectural Heritage*, 1-17, DOI: 10.1080/15583058.2020.1808911

[18] Ochsendorf, J. A. 2002. *Collapse of masonry structures*. PhD thesis. University of Cambridge.

[19] Ochsendorf, J. A. 2006. The masonry arch on spreading supports. *Structural Engineer*, 84 (2), 29–35.

[20] Smars, P., S. Pierre. 2010. Kinematic stability of masonry arches. *Advanced Materials Research*, 133–134, 429–434.

[21] Masciotta, M.G., D. Pellegrini, M. Girardi, C. Padovani, A. Barontini, P.B. Lourenco, D. Brigante, G. Fabbrocino. 2020. Dynamic characterization of progressively damaged segmental masonry arches with one settled support: experimental and numerical analyses. *Frattura ed Integrità Strutturale*, 51: 423-441. DOI: 10.3221/IGF-ESIS.51.31

[22] Shapiro, E.E. 2012. *Collapse mechanism of small-scale unreinforced masonry vaults*. M.S. Thesis in Building Technology, Massachusetts Institute of Technology, June 2012.

[23] Rossi, M., C. Calderini, S. Lagomarsino. 2016. Experimental testing of the seismic in-plane displacement capacity of masonry cross vaults through a scale model. *Bulletin of Earthquake Engineering*, 14(1): 261–281. DOI:10.1007/s10518-015-9815-1.

[24] D'Altri, A.M., S. De Miranda, G. Castellazzi, V. Sarhosis, J. Hudson, D. Theodossopoulos. 2019. Historic barrel vaults undergoing differential settlements, *International Journal of Architectural Heritage*, DOI:10.1080/15583058.2019.1596332

[25] Quinonez, A., J. Zessin, J.M. Ochsendorf. 2010. Small-Scale Models for the Analysis of Masonry Structures. *Proc. of the 7th International Conference on Structural Analysis of Historical Construction*. P.B. Lourenço, P. Roca (ed.), Shanghai.

[26] Carfagnini C., S. Baraccani, S. Silvestri, D. Theodossopoulos. 2018. The effects of in-plane shear displacements at the springings of Gothic cross vaults. *Construction and Building Materials*, 186: 219-232. DOI: 10.1016/j.conbuildmat.2018.07.055.

[27] Van Mele, T., J. McInerney, M. DeJong, P. Block. 2012. Physical and computational discrete modeling of masonry vault collapse, *Proc. of the 8th International Conference on Structural Analysis of Historical Constructions*, Wroclaw.

[28] Rossi, M., C. Calvo Barentin, T. Van Mele and P. Block. 2017. Experimental study on the behaviour of masonry pavilion vaults on spreading supports, *Structures*, 11:110-120. DOI: 10.1016/j.istruc.2017.04.008.

[29] Eslami, A., H.R. Ronagh, S.S. Mahini, R. Morshed. 2012. Experimental investigation and nonlinear FE analysis of historical masonry buildings – A case study, *Construction and Building Materials*, 35:251-260. DOI: 10.1016/j.conbuildmat.2012.04.002.

[30] Ferrero, C., M. Rossi, P. Roca, C. Calderini. 2021. Experimental and numerical analysis of a scaled dry-joint arch on moving supports, *International Journal of Masonry Research and Innovation*, DOI: 10.1504/IJMRI.2021.10035577

[31] Ferrero, C., C. Calderini, P. Roca. 2022. Experimental response of a scaled dry-joined masonry arch subject to inclined support displacement. *Engineering Structures*, 253: 113804. DOI 10.1016/j.engstruct.2021.113804.

[32] Baraccani, S., L. Zauli, D. Theodossopoulos, S. Silvestri. 2020. Experimental test on a fibre-reinforced scaled cross vault subjected to in-plane shear displacement at the springings, *Construction and Building Materials*, 265: 120305. DOI: 10.1016/j.conbuildmat.2020.120305.

575 [33] Romano A. 2005. *Modelling, analysis and testing of masonry structures*. PhD Thesis, University of Naples
576 Federico II.

577 [34] Theodossopoulos, D., B.P. Sinha, A.S. Usmani, A.J. Macdonald. 2002. Assessment of the structural
578 response of masonry cross vaults. *Strain*, 38: 119-127.

579 [35] Milani, G., M. Rossi, C. Calderini, S. Lagomarsino. 2016. Tilting plane tests on a small-scale masonry
580 cross vault: Experimental results and numerical simulations through a heterogeneous approach.
581 *Engineering Structures*, 123: 300–312. DOI: 10.1016/j.engstruct.2016.05.017.

582 [36] Calvo Barentin, C., T. Van Mele, P. Block. 2017. Robotically controlled scale-model testing of masonry
583 vault collapse, *Meccanica*, 53(7): 1917 – 1929. DOI: 10.1007/s11012-017-0762-6.

584 [37] Calderini, C., S. Lagomarsino. 2014. Seismic response of masonry arches reinforced by tie-rods: static tests
585 on a scale model. *Journal of Structural Engineering,* DOI: 10.1061/(ASCE)ST.1943-541X.0001079,
586 04014137.

587 [38] Marini, A., G. Giardina, P. Riva, E. Giurani. 2008. Seismic behaviour of barrel vault system. *Structural*
588 *Analysis of Historic Construction*, D'Ayala & Fodde (eds), Taylor & Francis Group, London, ISBN 978-
589 0-415-46872-5: 517-524.

590 [39] Albuerne, A., M. Williams. 2015. Monitoring the seismic response of arch models using particle image
591 velocimetry. *SECED 2015: Earthquake Risk and Engineering towards a Resilient World*.

592 [40] Williams, M.S., A. Albuerne, V. Lawson, F. Yip. 2012. Model scale shaking table tests on masonry barrel
593 and cross vaults. *Proc. of the 15th World Conference on Earthquake Engineering*, Lisbon.

594 [41] Bianchini, N., N. Mendes, P. Candeias, M. Rossi, C. Calderini, P. Lourenço, A. Campos Costa. 2020.
595 Seismic performance of masonry cross vaults through shaking table testing on a scaled model. *Proc. 12th*
596 *International Conference on Structural Analysis of Historical Constructions - SAHC 2020*, Barcelona.

597 [42] Calderini, C., S. Lagomarsino, M. Rossi, G. Decanio, M. Mongelli, I. Roselli. 2014. Shaking table tests of
598 an arch-pillars system and design of strengthening by the use of tie-roads. *Bulletin of Earthquake*
599 *Engineering*, DOI: 10.1007/s10518-014-9678-x.

600 [43] Gaetani, A., P.B. Lourenço, G. Monti, M. Moroni. 2017. Shaking table tests and numerical analyses on a
601 scaled dry-joint arch undergoing windowed sine pulses. *Bulletin of Earthquake Engineering*, 15(88): 1–23.
602 DOI: 10.1007/s10518-017-0156-0.

603 [44] European Committee for Standardization, UNI EN 12620, Aggregates for concrete, Brussels, 2008.

604 [45] Niezrecki, C., Baqersad, J., Sabato, A. 2018. *Digital Image Correlation techniques for non-destructive*
605 *evaluation and Structural Health Monitoring*, in Handbook of Advanced Non-Destructive Evaluation, Ida,
606 N., Meyendorf, N. (edited by), Springer, Cham, pp.1-46.

607 [46] Pierré, J.E., J.C. Passieux, J.N. Perié'. 2017. Finite Element Stereo Digital Image Correlation: framework
608 and mechanical regularization. *Experimental Mechanics*, 57:443–456. DOI: 10.1007/s11340-016-0246-y.

609 [47] Luhmann, T., S. Robson, S. Kyle, J. Bohem. 2013. *Close-Range Photogrammetry and 3D Imaging*, De
610 Gruyter, Berlin/Boston.

611 [48] Guidi, G., J. Beraldin, S. Ciofi, C. Atzeni. 2003. Fusion of range camera and photogrammetry: a systematic
612 procedure for improving 3-D models metric accuracy, *Ieee Transactions on Systems, Man, and Cybernetics*
613 *- Part B: Cybernetics*, 33(4): 667 - 676. DOI: 10.1109/TSMCB.2003.814282.

614 [49] Patrucco, G., F. Rinaudo, A. Spreafico. 2019. A new handheld scanner for 3d survey of small artifacts: the
615 Stonex F6, *The International Archives of the Photogrammetry, Remote Sensing and Spatial Information*
616 *Sciences*, XLII-2/W15: 895–901. DOI: 10.5194/isprs-archives-XLII-2-W15-895-2019.

[50] Malik, U.S., G. Guidi. 2018. Massive 3D digitation of sculptures: Methodological approaches for improving efficiency, *IOP Conference Series: Materials, Science and Engineering*, 364: 012015. DOI: 10.1088/1757-899X/364/1/012015.

[51] Georgopoulos A., Ioannidis C., Valanis A., 2010. Assessing the performance of a structured light scanner. *The International Archives of Photogrammetry, Remote Sensing and Spatial Information Sciences*, XXXVIII, Part 5 Commission V Symposium, Newcastle upon Tyne, UK: 250-255.

[52] Alforno, M. 2021. *Investigation of the role of constructive aspects on the structural response of masonry vaults*, PhD Thesis, Politecnico di Torino.